Received: 14 November 2019 | Revised: 27 December 2020 | Accepted: 27 December 2020

DOI: 10.1002/fut.22190

RESEARCH ARTICLE

THE JOURNAL OF FUTURES MARKETS WILEY

Consistent and efficient pricing of SPX and VIX options under multiscale stochastic volatility

Jaegi Jeon[1] | **Geonwoo Kim**[2] | **Jeonggyu Huh**[3]

[1]Department of Mathematical Sciences, Seoul National University, Seoul, Republic of Korea

[2]School of Liberal Arts, Seoul National University of Science and Technology, Seoul, Republic of Korea

[3]Department of Statistics, Chonnam National University, Gwangju, Republic of Korea

Correspondence
Jeonggyu Huh, Department of Statistics, Chonnam National University, Gwangju 61186, Republic of Korea.
Email: huhjeonggyu@jnu.ac.kr

Funding information
National Research Foundation of Korea, Grant/Award Numbers: NRF-2017R1E1A1A03070886, NRF-2019R1F1A1058352, NRF-2019R1I1A1A01062911

Abstract

We provide consistent and efficient pricing for both Standard & Poor's 500 Index options and the Chicago Board Options Exchange's Volatility Index options under a multiscale stochastic volatility model. To capture the multiscale, our model adds a fast scale factor to Heston's volatility and we derive approximate analytic formulas for the options under the model. The analytic tractability can greatly improve the efficiency of calibration compared to fitting procedures using a numerical scheme. Our experiment using options data for 3 years shows that the model reduces about 20% of the errors for a single-scale model.

KEYWORDS

asymptotic method, efficient pricing, multiscale volatility, SPX option, VIX option

1 | INTRODUCTION

Volatility in the financial market is one of the most important measures for investors. The Volatility Index (VIX) of the Chicago Board Options Exchange (CBOE) was introduced as a measure to capture the volatility of the Standard & Poor's 500 Index (SPX) in 1993. The VIX was revised to be independent of any model in 2003. Since the revision, it has been calculated using SPX option prices and the SPX over the next 30 calendar-day period. Since the introduction of the VIX, the index has become a standard gauge of market fear, because the VIX and the SPX are negatively correlated. In addition, VIX options have received a lot of attention, as the popularity of the VIX has grown, and this interest in derivatives has led to the development of an appropriate pricing method for them.

It is noteworthy that many researchers have developed pricing methods for VIX options under the models originally proposed to price SPX options. This may be because an arbitrage relationship exists between the SPX option market and the VIX option market. In the early research period for VIX options, studies aimed to derive pricing formulas for VIX options under several one-factor affine jump-diffusion (AJD) models; Lin and Chang (2009), Lian and Zhu (2013), Lin and Chang (2010), Cheng et al. (2012), and Cont and Kokholm (2013). As is widely known, the one-factor AJD model has a special structure from a mathematical standpoint and often gives a pricing formula for SPX options as well as VIX options (refer Duffie et al., 2000). The models are highly desirable in the sense that they make it possible to evaluate the SPX options and the VIX options without arbitrage. However, it is recognized that the models have a variety of fundamental limitations. Primarily, the models cannot accommodate the multiscale property of volatility,

which highlights the necessity of multifactor affine diffusion models. Jumps are usually excluded in the models, but the models have been frequently found to be superior to the one-factor AJD models in the literature, such as Kaeck and Alexander (2012).

In this light, on the other hand, Gatheral (2008) proposed the double-mean-reverting (DMR) Heston model to capture the multiscale of volatility. However, it does not provide any pricing formula and totally depends on the Monte-Carlo simulation for pricing and calibration. Although the simulation method has been greatly improved in Bayer et al. (2013), the model still fails to suggest a viable solution to calibration using a large number of option prices. On the other hand, Fouque and Saporito (2018) proposed the Heston stochastic vol-of-vol model (Heston SVV model) with fast and slow time scales to reflect skews in both the SPX data and VIX data, and derived approximation solutions for the prices of options on the SPX and VIX, respectively. Moreover, the Heston SVV model calibrated jointly to real market data for the SPX and VIX was shown to fit the data very well. Their solutions, however, cannot be computed within a short period of time. Interestingly, Huh et al. (2018) obtained an approximate quasi-closed formula for VIX options under the DMR Heston model and furthermore confirmed with real market data that the calibration result utilizing the approximate solution is analogous to the case using simulation methods. However, the approach can be applied to pricing VIX options only.

Our novel model is the first multifactor affine diffusion model to give practically feasible pricing formulas for both SPX options and VIX options. Specifically, we propose a new two-factor affine diffusion model and induce approximate quasi-closed formulas for both the options based on the perturbation theory. The analytic tractability greatly improves the efficiency of calibration. As a result, we achieve satisfactory calibration results with long-term data for the SPX and VIX from 2016 to 2018, consisting of hundreds of thousands of options.

The remainder of the paper is organized as follows. We introduce a new two-factor model with multiscale volatility to jointly price VIX options and SPX options in Section 2. We derive the analytic pricing formulas of SPX options and VIX options under the proposed model using asymptotic methods in Section 3. We present calibration with real options data for the SPX and VIX in Section 4. We provide concluding remarks in Section 5.

2 | A NEW TWO-FACTOR MULTISCALE STOCHASTIC VOLATILITY MODEL

Before introducing our model, we briefly review the double Heston model of Christoffersen et al. (2009). The model was originally devised to reflect stochastic correlation as well as stochastic volatility. The improvement is achievable because the model has two factors for volatility. By contrast, the Heston model cannot capture stochastic correlation because it has only one factor for volatility. The double Heston model, however, cannot capture the multiscale characteristics of a market, because it was not designed for this purpose (see Chernov et al., 2003; Gallant et al., 1999). Thus, the model needs to be extended to depict well-separated time scales. More importantly, the model provides an analytic formula for VIX options, which requires heavy computation for a double integral. In particular, when practitioners want to fit the model to prices for both SPX options and VIX options consistently within a limited time, the time cost raises a severe problem.

To overcome these limitations of the double Heston model, we propose a two-factor multiscale stochastic volatility model, which is given by the following stochastic differential equations:

$$\begin{aligned} dX_t &= rX_t dt + \sqrt{Y_t} X_t dW_t^{X,1} + \sqrt{Z_t} X_t dW_t^{X,2}, \\ dY_t &= \frac{1}{\epsilon}(Z_t - Y_t)dt + \frac{\sqrt{2}\nu}{\sqrt{\epsilon}}\sqrt{Y_t} dW_t^{Y}, \\ dZ_t &= \kappa(\theta - Z_t)dt + \sigma\sqrt{Z_t} dW_t^{Z} \end{aligned} \tag{1}$$

for $0 < \epsilon \ll 1$ under a risk-neutral measure $\mathcal{Q}$, where r is the risk-free rate, and $\kappa \ll 1/\epsilon$ is assumed. The correlation structure of our model is

$$\begin{aligned} &dW_t^{X,1} dW_t^{Y} = \eta dt, \quad dW_t^{X,2} dW_t^{Z} = \rho dt, \\ &dW_t^{X,1} dW_t^{Z} = dW_t^{X,2} dW_t^{Y} = dW_t^{X,1} dW_t^{X,2} = dW_t^{Y} dW_t^{Z} = 0. \end{aligned}$$

It should be noted that Y_t rapidly reverts to Z_t under our model, which is a major difference with the double Heston model. Because the time scales are clearly separated due to condition $\kappa \ll 1/\epsilon$, the short-term variance $Y_t + Z_t$ rapidly

reverts to midterm variance $2Z_t$, and $2Z_t$ regresses to long-term variance 2θ at a relatively slow rate. On the other hand, one can consider that our model is obtained by adding a fast mean-reverting factor to Heston's volatility or otherwise by modifying the double Heston model to express the well-separated time scales.

3 | PRICING SPX AND VIX OPTIONS

3.1 | An approximate analytic formula for SPX options

By the risk-neutral pricing principle, the price P_s^ϵ for an SPX call option with strike K and maturity T at time t is

$$P_s^\epsilon(t,x,y,z) = e^{-r(T-t)}\mathrm{E}^{\mathbb{Q}}_{x,y,z}[(X_T - K)^+], \tag{2}$$

where $(X_t, Y_t, Z_t) = (x, y, z)$. Applying the Feynman–Kac theorem to our model (1), it can be shown that P_s^ϵ should satisfy the following partial differential equation (PDE):

$$\left(\frac{1}{\epsilon}\mathcal{L}_{s,0} + \frac{1}{\sqrt{\epsilon}}\mathcal{L}_{s,1} + \mathcal{L}_{s,2}\right)P_s^\epsilon(t,x,y,z) = 0,$$

where

$$\begin{aligned}
\mathcal{L}_{s,0} &= (z-y)\partial_y + \nu^2 y\partial^2_{yy},\\
\mathcal{L}_{s,1} &= \sqrt{2}\eta\nu xy\partial^2_{xy},\\
\mathcal{L}_{s,2} &= \partial_t + rx\partial_x + \kappa(\theta - z)\partial_z + \frac{1}{2}x^2(y+z)\partial^2_{xx} + \frac{1}{2}\sigma^2 z\partial^2_{zz} + \rho\sigma xz\partial^2_{xz} - r\cdot
\end{aligned} \tag{3}$$

with the final condition $P_s^\epsilon(T,x,y,z) = (x-K)^+$. Deriving an analytic solution for this PDE would be desirable; however, we confirm that the solution cannot be easily induced.

Thus, we attempt to obtain an approximate solution for P_s^ϵ based on asymptotic methods (refer to Fouque et al., 2011). Let us expand P_s^ϵ with respect to $\sqrt{\epsilon}$, that is, $P_s^\epsilon = P_{s,0} + \sqrt{\epsilon}P_{s,1} + \epsilon P_{s,2} + \cdots$. We wish to approximate P_s^ϵ to the sum of the leading term $P_{s,0}$ and the first nonzero correction term $P_{s,1}$. To do this, we show that $P_{s,0}$ and $P_{s,1}$ follow the following PDEs independent of y:

- leading term $P_{s,0}$

$$\begin{aligned}
\langle\mathcal{L}_{s,2}\rangle P_{s,0} &= 0,\\
P_{s,0}(T,x,z) &= (x-K)^+,
\end{aligned} \tag{4}$$

- first nonzero correction term $P_{s,1}$

$$\begin{aligned}
\langle\mathcal{L}_{s,2}\rangle P_{s,1} &= W_3^\epsilon zx\partial_x(x^2\partial_{xx})P_{s,0},\\
P_{s,1}(T,x,z) &= 0,
\end{aligned} \tag{5}$$

where

$$\begin{aligned}
\langle\mathcal{L}_{s,2}\rangle &= \partial_t + rx\partial_x + \kappa(\theta - z)\partial_z + x^2z\partial^2_{xx} + \frac{1}{2}\sigma^2 z\partial^2_{zz} + \rho\sigma xz\partial^2_{xz} - r,\\
W_3^\epsilon &= -\frac{1}{\sqrt{2}}\eta\nu\sqrt{\epsilon},
\end{aligned}$$

and $\langle\cdot\rangle$ is the expectation with respect to the invariant distribution Φ for Y_t, that is, $\langle f\rangle = \int f(y)\Phi(y)dy$. To be precise, $Y_\infty \sim \Gamma(\gamma, \nu^2)$, which means that the density function Φ for Y_∞ is given by

$$\Phi(w) = \frac{1}{\nu^{2\gamma}\Gamma(\gamma)}w^{\gamma-1}e^{-(w/\nu^2)}\mathbf{1}_{(0,\infty)}(w),$$

where $\gamma = \frac{z}{\nu^2}$. If setting $2z = \xi$, the operator $\langle \mathcal{L}_{s,2} \rangle$ changes to

$$\mathcal{L}_H = \partial_t + rx\partial_x + \kappa(2\theta - \xi)\partial_\xi + \frac{1}{2}x^2\xi\partial^2_{xx} + \frac{1}{2}(\sqrt{2}\sigma)^2\xi\partial^2_{\xi\xi} + \left(\frac{1}{\sqrt{2}}\rho\right)(\sqrt{2}\sigma)x\xi\partial^2_{x\xi} - r.$$

The resulting operator $\mathcal{L}_H$ can be then regarded as that generated from the Heston model whose parameters are the mean-reverting rate κ, the long-term variance level 2θ, the volatility of volatility $\sqrt{2}\sigma$, and the leverage correlation $\rho/\sqrt{2}$.

The analytic solutions for the PDEs can be obtained by exploiting the analytical tractability of affine models fully. In fact, the key idea for the derivation of the solutions is strongly motivated by the work of Fouque and Lorig (2011). However, under their model, the solutions for SPX options are involved in triple integrals requiring overly large computational resources. By contrast, it is proved that our solutions are all involved in single integrals. More importantly, they give a solution only for SPX options, but we provide consistent solutions for both SPX options and VIX options. The expressions for $P_{s,0}$ and $P_{s,1}$ are summarized in the following theorem.

Theorem 1. *The price P^ϵ_s in (2) can be approximated with an accuracy of order $O(\epsilon)$, that is,*

$$\left|P^\epsilon_s - (P_{s,0} + P_{s,1})\right| < C\epsilon$$

for some $C > 0$. Furthermore, $P_{s,0}$ and $P_{s,1}$ have the following forms:

$$P_{s,0}(t,x,z) = \frac{e^{-r\tau}}{2\pi}\int e^{-ikq}\hat{G}(\tau,k,2z)\hat{h}(k)dk,$$
$$P_{s,1}(t,x,z) = \frac{e^{-r\tau}}{2\pi}\int e^{-ikq}b(k)(\kappa\theta\hat{f}_0(\tau,k) + 2z\hat{f}_1(\tau,k))\hat{G}(\tau,k,2z)\hat{h}(k)dk,$$

where $\tau = T - t$, $q = r\tau + \log x$,

$$\hat{G}(\tau,k,y) = e^{C(\tau,k)+yD(\tau,k)},$$
$$\hat{h}(k) = \frac{K^{1+ik}}{ik - k^2},$$
$$\hat{f}_0(\tau,k) = \frac{2\tau d(k)g(k) + g^2(k) - 1}{d^2(k)g(k)(g(k)e^{\tau d(k)} - 1)} + \frac{\tau d(k)g(k) - g(k) - 1}{d^2(k)g(k)},$$
$$\hat{f}_1(\tau,k) = \frac{e^{\tau d(k)}(g(k)^2(e^{\tau d(k)} - 1) - 2\tau d(k)g(k) + 1) - 1}{d(k)(g(k)e^{\tau d(k)} - 1)^2},$$

and

$$C(\tau,k) = \frac{\kappa\theta}{\sigma^2}\left((\kappa + \rho ik\sigma - d(k))\tau - 2\log\left(\frac{e^{-\tau d(k)} - g(k)}{1 - e^{-\tau d(k)}g(k)}\right)\right),$$
$$D(\tau,k) = \frac{\kappa + \rho ik\sigma + d(k)}{2\sigma^2}\left(\frac{e^{-\tau d(k)} - 1}{e^{-\tau d(k)} - g(k)}\right),$$
$$b(k) = -\frac{1}{2}W^\epsilon_3(ik^3 + k^2),$$
$$d(k) = \sqrt{2\sigma^2(k^2 - ik) + (\kappa + \rho ik\sigma)^2},$$
$$g(k) = \frac{\kappa + \rho ik\sigma + d(k)}{\kappa + \rho ik\sigma - d(k)}.$$

Proof. The detailed proof is in Appendix A. □

3.2 | Relationship between the VIX and our model

Before proceeding, we show the relationship between the VIX[1] and our model. Because the VIX at time t, VIX_t^ϵ, is the square root of an integration of spot variance from t to $t+\tau_0(\tau_0 := 30/365)$, based on Carr and Madan (1998), the relationship can be given by

$$\begin{aligned}\left(\mathrm{VIX}_t^\epsilon\right)^2 &= 100^2 \times \mathrm{E}^{\mathcal{Q}}\left[\frac{1}{\tau_0}\int_t^{t+\tau_0}(Y_s+Z_s)ds\right]\\ &= 100^2 \times \frac{1}{\tau_0}\int_t^{t+\tau_0}(\mathrm{E}^{\mathcal{Q}}[Y_s]+\mathrm{E}^{\mathcal{Q}}[Z_s])ds\\ &= 100^2 \times \left(a_1^\epsilon Y_t + a_2^\epsilon Z_t + \left(a_3^\epsilon + a_4^\epsilon\right)\theta\right),\end{aligned} \tag{6}$$

where

$$\begin{aligned}a_1^\epsilon &= \frac{\epsilon}{\tau_0}\left(1-e^{-\tau_0/\epsilon}\right),\\ a_2^\epsilon &= \frac{1}{\kappa\tau_0}\left(1-e^{-\kappa\tau_0}\right)+\frac{1}{1-\kappa\epsilon}\left(\frac{1}{\kappa\tau_0}\left(1-e^{-\kappa\tau_0}\right)-\frac{\epsilon}{\tau_0}\left(1-e^{-\tau_0/\epsilon}\right)\right),\\ a_3^\epsilon &= 1-a_1^\epsilon,\\ a_4^\epsilon &= 1-a_2^\epsilon.\end{aligned}$$

The following facts induced by Ito's lemma are used for the derivation of the above formula (6).

$$\begin{aligned}\mathrm{E}[Y_s] &= e^{-\frac{1}{\epsilon}(s-t)}Y_t + \frac{1}{1-\kappa\epsilon}\left(e^{-\kappa(s-t)}-e^{-\frac{1}{\epsilon}(s-t)}\right)Z_t\\ &\quad+\left[\left(1-e^{-\frac{1}{\epsilon}(s-t)}\right)-\frac{1}{1-\kappa\epsilon}\left(e^{-\kappa(s-t)}-e^{-\frac{1}{\epsilon}(s-t)}\right)\right]\theta,\\ \mathrm{E}[Z_s] &= e^{-\kappa(s-t)}Z_t+\theta(1-e^{-\kappa(s-t)}).\end{aligned}$$

It is noteworthy that $\left(\mathrm{VIX}_t^\epsilon\right)^2$ converges surely to

$$\left(\mathrm{VIX}_t^*\right)^2 = 100^2 \times \left(a_2^* Z_t + \left(1+a_4^*\right)\theta\right),$$

as $\epsilon \to 0$, because $a_1^\epsilon \to 0$, $a_2^\epsilon \to a_2^* := \frac{2}{\kappa\tau_0}\left(1-e^{-\kappa\tau_0}\right)$, $a_3^\epsilon \to 1$, and $a_4^\epsilon \to a_4^* := 1-a_2^*$ pointwise as $\epsilon \to 0$. In addition, VIX_t and VIX_t^* have the following relationship:

$$\left(\mathrm{VIX}_t^\epsilon\right)^2-\left(\mathrm{VIX}_t^*\right)^2 = 100^2 \times \left(\frac{\epsilon}{\tau_0}\left(1-e^{-\tau_0/\epsilon}\right)(Y_t-Z_t)+\frac{\epsilon}{\tau_0}\left(1-e^{-\kappa\tau_0}\right)(Z_t-\theta)\right)+O(\epsilon^2) := \Delta\mathrm{VIX}_t^2.$$

3.3 | An approximate analytic formula for VIX options

Denoting the price for a VIX call option with strike K and maturity T at time t as P_v^ϵ, P_v^ϵ is expressed by

$$P_v^\epsilon(t,y,z) = e^{-r(T-t)}\mathrm{E}_{y,z}^{\mathcal{Q}}[h^\epsilon(Y_T,Z_T)], \tag{7}$$

where $(Y_t,Z_t)=(y,z)$, and $h^\epsilon(u,v)=\left(\mathrm{VIX}_T^\epsilon(u,v)-K\right)^+$. If $H(x) := (\sqrt{x}-K)^+$, $h^\epsilon(u,v)=H\left(\left(\mathrm{VIX}_T^\epsilon\right)^2\right)$. Then, by expanding H at $\left(\mathrm{VIX}_t^*\right)^2$, h^ϵ can be transformed to

[1] http://www.cboe.com/micro/vix/vixwhite.pdf

$$
\begin{aligned}
h^{\epsilon}(u,v) &= H\left(\left(\mathrm{VIX}_T^*\right)^2\right) + H'\left(\left(\mathrm{VIX}_T^*\right)^2\right)\Delta\mathrm{VIX}_t^2 + \frac{1}{2}H''\left(\left(\mathrm{VIX}_T^*\right)^2\right)\left(\Delta\mathrm{VIX}_t^2\right)^2 + \cdots \\
&= \left(\sqrt{a_2^* v + \left(1+a_4^*\right)\theta} \times 100 - K\right)\mathbf{1}_{\left\{v \geq \left(K^2 - \left(1+a_4^*\right)\theta\right)/a_2^*\right\}} \\
&\quad + \epsilon\left(\frac{(1-e^{-\tau_0/\epsilon})(u-v) + (1-e^{-\kappa\tau_0})(v-\theta)}{2\tau_0\sqrt{a_2^* v + \left(1+a_4^*\right)\theta}}\right)\mathbf{1}_{\left\{v \geq \left(K^2 - \left(1+a_4^*\right)\theta\right)/a_2^*\right\}} \times 100 + O(\epsilon^2) \\
&= h_0(v) + \epsilon h_1(u,v) + O(\epsilon^2),
\end{aligned}
$$

where h_0 and h_1 are the first and second terms of the second line, respectively. Meanwhile, utilizing Ito's lemma, we can show

$$
\begin{aligned}
Y_s &= Z_s + e^{-\frac{1}{\epsilon}(s-t)}(Y_t - Z_t) + \frac{\sqrt{2}\nu}{\sqrt{\epsilon}}\int_t^s e^{-\frac{1}{\epsilon}(s-u)}\sqrt{Y_u}\,dW_u^Y \\
&\quad + \sum_{n=1}^{\infty}(\kappa\epsilon)^n\left[(Z_s - \theta) - e^{-\frac{1}{\epsilon}(s-t)}(Z_t - \theta)\right] - \sigma\sum_{n=0}^{\infty}(\kappa\epsilon)^n\int_t^s e^{-\frac{1}{\epsilon}(s-u)}\sqrt{Z_u}\,dW_u^Z.
\end{aligned}
$$

Using the tower property of conditional expectation and the linearity of h_1 with respect to u, we obtain

$$
\begin{aligned}
\mathrm{E}_{y,z}^{\mathcal{Q}}[h(Y_T, Z_T)] &= \mathrm{E}_{y,z}^{\mathcal{Q}}\left[\mathrm{E}_{y,z}^{\mathcal{Q}}[h(Y_T, Z_T)|Z_T]\right] \\
&= \mathrm{E}_{y,z}^{\mathcal{Q}}\left[\mathrm{E}_{y,z}^{\mathcal{Q}}[h_0(Z_T) + \epsilon h_1(Y_T, Z_T)|Z_T]\right] + O(\epsilon^2) \\
&= \mathrm{E}_{y,z}^{\mathcal{Q}}\left[h_0(Z_T) + \epsilon h_1\left(\mathrm{E}_{y,z}^{\mathcal{Q}}[Y_T|Z_T], Z_T\right)\right] + O(\epsilon^2) \\
&= \mathrm{E}_{y,z}^{\mathcal{Q}}[h_0(Z_T) + \epsilon h_1(Z_T + e^{-(T-t)/\epsilon}(y-z) + O(\epsilon), Z_T)] + O(\epsilon^2) \\
&= \mathrm{E}_{y,z}^{\mathcal{Q}}\left[h_0(Z_T) + h_1^*(Z_T)\right] + O(\epsilon^2),
\end{aligned}
$$

where $h_1^*(v) = \epsilon h_1(v + e^{-(T-t)/\epsilon}(y-z), v)$. Then, the facts presented so far lead to the following theorem.

Theorem 2. *The price P_v^{ϵ} in (7) can be approximated with accuracy of order $O(\epsilon^2)$, that is,*

$$
\left|P_v^{\epsilon} - (P_{v,0} + P_{v,1})\right| < C\epsilon^2.
$$

for some $C > 0$. Furthermore, $P_{v,0}$ and $P_{v,1}$ are given by

$$
\begin{aligned}
P_{v,0}(t,z) &= e^{-rT}\int_0^{\infty} h_0(\delta\zeta)\, f(\zeta; k, \lambda)\, d\zeta, \\
P_{v,1}(t,y,z) &= e^{-rT}\int_0^{\infty} h_1^*(\delta\zeta)\, f(\zeta; k, \lambda)\, d\zeta,
\end{aligned}
$$

where $f(\zeta; k, \lambda)$ is the density function of a noncentral χ^2 distribution with $k = \frac{4\kappa\theta}{\sigma^2}$ degrees of freedom and noncentrality parameter $\lambda = \frac{ze^{-\kappa\tau}}{\delta}$ with $\tau = T - t$, where $\delta = \frac{(1-e^{-\kappa\tau})\sigma^2}{4\kappa}$, and

$$
\begin{aligned}
h_0(v) &= \left(\sqrt{a_2^* v + \left(1+a_4^*\right)\theta} \times 100 - K\right)^+ \mathbf{1}_{\{v \geq (K^2 - (1+a_4^*)\theta)/a_2^*\}}, \\
h_1^*(v) &= \epsilon\left(\frac{2e^{-\tau/\epsilon}a_1^{\epsilon}(y-z) + \kappa\epsilon a_2^*(v-\theta)}{4\sqrt{a_2^* v + (1+a_4^*)\theta}}\right)\mathbf{1}_{\{v \geq (K^2 - (1+a_4^*)\theta)/a_2^*\}} \times 100.
\end{aligned}
$$

Proof. Because it is known that future values of the Cox–Ingersoll–Ross (CIR) process Z_t follow a noncentral χ^2 distribution, the values of $P_{v,0}$ and $P_{v,1}$ can be expressed as the expectations with respect to the distribution (c.f. Brigo & Mercurio, 2007). □

Note that the above analytic formulas in Theorem 2 are involved in single Integrals, as in the case of the formulas for SPX options. This means that it is possible to compute the values without difficulty. We also strongly stress that our model has only six parameters $\kappa, \theta, \sigma, \rho, \epsilon$, and W_3^ϵ, which is only two more than the Heston model. Some of the parameters $\left(W_3^\epsilon, \rho\right)$ and ϵ control only of SPX and VIX option prices, respectively.

4 | EMPIRICAL TEST

In this section, we verify the outperformance of our two-factor stochastic volatility model (SV2) through an empirical test using real market data. To show the benefits of the SV2 clearly, we compare it with the one-factor stochastic volatility model (SV1) reduced from the SV2, for which the prices of the SPX and VIX options are given by $P_{s,0}$ and $P_{v,0}$ in (1) and (2), respectively. Recall that the those of the SV2 correspond to $P_{s,0} + \sqrt{\epsilon} P_{s,1}$ and $P_{v,0} + \epsilon P_{v,1}$ in (1) and (2), respectively. While it may be considered more reasonable to compare our model with another two-factor stochastic volatility model, there is no existing two-factor stochastic volatility model that gives analytic pricing formulas that are available and efficient for both SPX and VIX options. For example, the double Heston model (Christoffersen et al., 2009) provides a double integral form for the pricing of VIX options but cannot be considered in practice because it takes a huge amount of time to compute, as its parameters are found based on a lot of option prices.

We obtain options data on the SPX and the VIX from 2016 to 2018 from the CBOE DataShop.[2] We filter them out if their daily trades are below 50, if their prices do not reach 0.5 point, or if they expire within 3 days. We then split the data into a training set for 2016–2017 (220,222 SPX options and 44,173 VIX options) and a test set for 2018 (165,309 SPX options and 22,116 VIX options). Figure 1 shows the series of the SPX and the VIX for the data period. The vertical red line indicates the dividing date, the left and the right of which correspond to the training period and the test period, respectively. Many financial crises arose during the period: Chinese stock market turbulence (early 2016), Brexit (late 2016), and U.S. stock market downturn (2018). It is clear that the SPX falls sharply and the VIX increases dramatically during each crisis. Table 1 summarizes the moments for the log-returns of both series for the data period. The VIX returns move in a much more volatile way than the SPX returns move. In addition, the SPX returns show negative skewness and weak kurtosis (>3), while the VIX returns show positive skewness and strong kurtosis (>>3). These findings imply that VIX options tend to be more expensive and riskier than SPX options are.

As in Broadie et al. (2007), we aim to minimize the root mean square errors (RMSE) between the model and market-implied volatilities, which is called IV-RMSE usually. This loss function avoids heavy weighting of a specific class of options, such as in-the-money options, expressed by

$$L^{IV}(\{z_i\}_{i\in I}; \Theta_\alpha) = \sqrt{\left\{L_s^{IV}(\{z_i\}_{i\in I}; \Theta_\alpha)\right\}^2 + \left\{L_v^{IV}(\{z_i\}_{i\in I}; \Theta_\alpha)\right\}^2} \tag{8}$$

such that the market-observed quantity VIX_i^{mkt} matches the model-based $\mathrm{VIX}_{i,\alpha}^{mdl}$, namely,

$$\mathrm{VIX}_i^{mkt} = \mathrm{VIX}_{i,\alpha}^{mdl}(y_i, z_i; \Theta_\alpha), \tag{9}$$

where

$$L_\gamma^{IV}(\{z_i\}_{i\in I}; \Theta_\alpha) = \sqrt{\frac{\beta_\gamma}{N_\gamma} \sum_{i\in I} \sum_{j\in J_{\gamma,i}} \left(\sigma_\gamma^{mdl}(z_i, \Theta_\alpha; t_i, K_j, T_j) - \sigma_\gamma^{mkt}(t_i, K_j, T_j)\right)^2},$$

σ^{mkt} and σ^{mdl} stand for the implied volatilities of the market and model prices, respectively, γ and α are indicators for the type of underlying assets and models, respectively, $\gamma \in \{s, v\}$, $\alpha \in \{\mathrm{SV1}, \mathrm{SV2}\}$, s and v represent the SPX and the VIX, respectively, β_γ is constant to balance the weights of the two terms L_s^{IV} and L_v^{IV}, and N_γ is the total number of options

[2] https://DataShop.cboe.com/

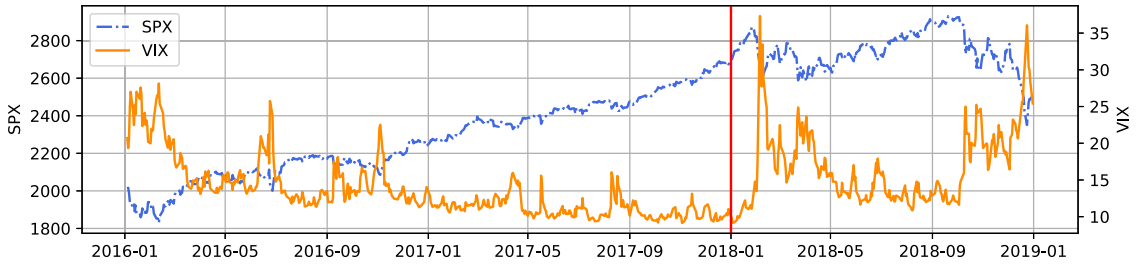

FIGURE 1 Series of the SPX and the VIX for 2016–2018. The vertical red line indicates the dividing date, the left and the right of which correspond to the training period (2016–2017) and the test period (2018), respectively. SPX, Standard & Poor's 500 Index; VIX, volatility index [Color figurecan be viewed at wileyonlinelibrary.com]

whose underlying asset corresponds to γ. I is the index set of the dates for the training set, and $J_{v,i}$ and $J_{s,i}$ are the index sets of the VIX options and the SPX options, respectively, on the ith date. In addition, $\mathrm{VIX}^{mdl}_{i,\mathrm{SV}\,1}(y_i) = \sqrt{b_2^* z_i + b_4^* \theta}$, $\mathrm{VIX}^{mdl}_{i,\mathrm{SV}\,2}(y_i, z_i) = \sqrt{a_1^{\epsilon} y_i + a_2^{\epsilon} z_i + \left(a_3^{\epsilon} + a_4^{\epsilon}\right)\theta}$, $\Theta_{\mathrm{SV}\,1} = \{\kappa, \theta, \sigma, \rho\}$, $\Theta_{\mathrm{SV}\,2} = \{\kappa, \theta, \sigma, \rho, \epsilon, W_3\}$, where $b_2^* = a_2^*/2$ and $b_4^* = \left(1 + a_4^*\right)/2$.

However, this approach has a severe problem. The Black–Scholes model has only one parameter $\sigma > 0$, and thus, it can provide a theoretical foundation for the implied volatility for SPX options. However, there is no model to perform a similar role for VIX options. Thus, to create the notion of implied volatility for VIX options consistently, we invent the following simple model:

$$d\mathrm{VIX}_t = \psi(t)dt + \sigma dW_t,$$

where $\sigma > 0$, $\int_{t.}^{u} \psi(s)ds = \mathrm{VIX}_t^u$, and VIX_t^u is the future price with maturity u at time t ($u \geq t$). This model implies $\mathrm{VIX}_T = \mathrm{VIX}_t^T + \sigma(W_T - W_t)$, that is, $\mathrm{VIX}_T \sim N\left(\mathrm{VIX}_t^T, \sigma\sqrt{T-t}\right)$. It is then easy to show that price $\tilde{P}_v^{call}$ of a VIX call option with maturity T and strike K is given by

$$\tilde{P}_v^{call}\left(\mathrm{VIX}_t^T; \sigma\right) = \left(\mathrm{VIX}_t^T - K\right)N\left(\frac{\mathrm{VIX}_t^T - K}{\sigma\sqrt{T-t}}\right) + \sigma\sqrt{T-t}\quad n\left(\frac{\mathrm{VIX}_t^T - K}{\sigma\sqrt{T-t}}\right), \tag{10}$$

where N and n are the cumulative distribution function and the probability density function of the unit Gaussian distribution, respectively. The pricing formula for a VIX put option can be obtained as follows:

$$\tilde{P}_v^{put}\left(\mathrm{VIX}_t^T; \sigma\right) = \tilde{P}_v^{call}\left(\mathrm{VIX}_t^T\right) - \left(\mathrm{VIX}_t^T - K\right). \tag{11}$$

As a result, for a market price P_v^{mkt}, the implied volatility for a VIX option can be defined as σ in (10) and (11) to match the model price $\tilde{P}_v^{mdl}$ with P_v^{mkt}. Note that, if denoting the payoff of an option as g, $\tilde{P}_v = \mathrm{E}^{\mathcal{Q}}[g(\mathrm{VIX}_T)] \geq g(\mathrm{E}^{\mathcal{Q}}[\mathrm{VIX}_T]) = g\left(\mathrm{VIX}_t^T\right)$ owing to Jensen's inequality. This implies that, if regarding the

TABLE 1 Moments for the log-return series of the SPX and the VIX

	SPX				VIX			
	Mean	***SD***	**Skewness**	**Kurtosis**	**Mean**	***SD***	**Skewness**	**Kurtosis**
Training	0.001	0.007	−0.530	4.379	−0.001	0.073	0.816	6.230
Test	0.000	0.011	−0.435	3.319	0.004	0.100	2.170	13.289
All	0.000	0.008	−0.581	5.295	0.000	0.083	1.669	12.385

Note: This presents the moments for the log-returns of both series for the data period from 2016 to 2018.

Abbreviations: SPX, Standard & Poor's 500 Index; VIX, volatility index.

TABLE 2 The point estimates, and the standard errors and correlations between the estimates, and V-RMSEs on the test data

(a) The point estimates and the $\mathcal{V}$-RMSEs on the test data

	Parameter estimates						$\mathcal{V}$-RMSE	
	κ	θ	σ	ρ	ϵ	W_3	SPX	VIX
SV1	1.62	0.0294	0.284	−1			0.04482	0.10002
	(0.18)	(0.0021)	(0.008)	(0.165)				
SV2	1.49	0.0302	0.260	−1	0.0245	−0.0089	0.03788	0.07629
	(0.25)	(0.0024)	(0.009)	(0.086)	(0.0023)	(0.0013)		
Error ratio							84.50%	76.28%

(b) The correlation of estimates for the SV1

	κ	θ	σ	ρ
κ	1.00	−0.98	0.68	−0.02
θ		1.00	−0.60	0.01
σ			1.00	−0.07
ρ				1.00

(c) The correlation of estimates for the SV2

	κ	θ	σ	ρ	ϵ	W_3
κ	1.00	−0.98	0.83	−0.38	−0.32	0.51
θ		1.00	−0.74	0.37	0.22	−0.50
σ			1.00	−0.32	−0.46	0.44
ρ				1.00	0.15	−0.51
ϵ					1.00	−0.15
W_3						1.00

Note: These tables show the point estimates, and the standard errors and correlations between the estimates, and $\mathcal{V}$-RMSEs on the test data for the SV1 and SV2 when $\beta_s = 1$ and $\beta_v = 0.0002$ in (13). The error ratio means the value obtained by dividing the error for the SV2 by the corresponding error for the SV1.

Abbreviations: RMSE, root mean square error; SPX, Standard & Poor's 500 Index; SV, stochastic volatility; VIX, volatility index.

underlying asset of the option as VIX_t^T, the time value $\tilde{P}_v - g\left(\mathrm{VIX}_t^T\right)$ of the option is always nonnegative. Thus, the implied volatility for VIX options is well defined for any strike prices.

In fact, even if we consistently define the implied volatility for VIX options, the computation for the loss (8) is fairly costly, because $\sigma_\gamma^{mdl}(K_j, T_j)$ has to be computed from $P_\gamma^{mdl}(K_j, T_j)$ at each step of a numerical optimization. The vega RMSE ($\mathcal{V}$-RMSE), an accurate approximation of the IV-RMSE, is often utilized to circumvent this difficulty. The following loss function $L^{\mathcal{V}}$ is the $\mathcal{V}$-RMSE:

$$L^{\mathcal{V}}(\{z_i\}_{i\in I};\Theta_\alpha) = \sqrt{\left\{L_s^{\mathcal{V}}(\{z_i\}_{i\in I};\Theta_\alpha)\right\}^2 + \left\{L_v^{\mathcal{V}}(\{z_i\}_{i\in I};\Theta_\alpha)\right\}^2} \tag{12}$$

such that

$$\mathrm{VIX}_i^{mkt} = \mathrm{VIX}_{i,\alpha}^{mdl}(y_i, z_i;\Theta_\alpha),$$

where

$$\begin{aligned} L_\gamma^{\mathcal{V}}(\{z_i\}_{i\in I};\Theta_\alpha) &= \sqrt{\frac{\beta_\gamma}{N_\gamma}\sum_{i\in I}\sum_{j\in J_{\gamma,i}}\left(e_{i,j}^{\mathcal{V}}\right)^2} \\ &= \sqrt{\frac{\beta_\gamma}{N_\gamma}\sum_{i\in I}\sum_{j\in J_{\gamma,i}}\left(\frac{P_\gamma^{mdl}(z_i,\Theta_\alpha;t_i,K_j,T_j) - P_\gamma^{mkt}(t_i,K_j,T_j)}{\delta + \mathcal{V}_\gamma^{mkt}(t_i,K_j,T_j)}\right)^2}, \end{aligned} \tag{13}$$

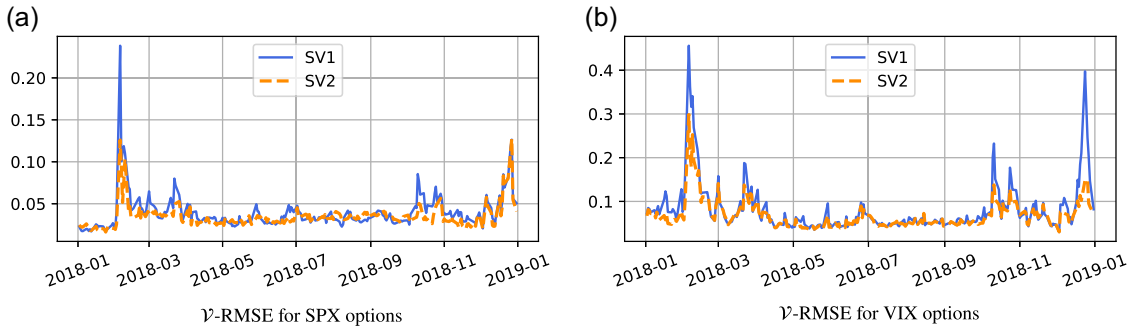

FIGURE 2 Comparison of daily $\mathcal{V}$-RMSE of both models by product types during the period of the test data (2016–2018) (a) $\mathcal{V}$-RMSE for SPX options; (b) $\mathcal{V}$-RMSE for VIX options. RMSE, root mean square error; SPX, Standard & Poor's 500 Index; VIX, volatility index [Color figurecan be viewed at wileyonlinelibrary.com]

$\mathcal{V}_s^{mkt}$ is the Black–Scholes vega on P_s^{mkt}, that is, $\mathcal{V}_s^{mkt} = \partial P_{BS}(\sigma)/\partial\sigma\,|_{\sigma=\sigma_s^{mkt}}$, $P_{BS}(\sigma)$ is the Black–Scholes price for the volatility σ, and $\mathcal{V}_v^{mkt}$ is the sensitivity of $\tilde{P}_v$ with respect to σ on P_v^{mkt}, that is, $\mathcal{V}_v^{mkt} = \partial\tilde{P}_v(\sigma)/\partial\sigma\,|_{\sigma=\sigma_v^{mkt}}$. In addition, $\delta = 0.01 \times P_\gamma^{mkt}(t_i, K_j, T_j)$, which is meant to stabilize the objective function. When analyzing real data, we sometimes obtain unreasonable σ^{mkt} or $\mathcal{V}^{mkt}$, such as almost zero values. This is because the last trade in an option and the corresponding underlying asset and future are not made at exactly the same time. Thus, we exclude the options that have the bottom 2% of σ^{mkt} and the bottom 5% of $\mathcal{V}^{mkt}$. Furthermore, it is noteworthy that our work is the first study to optimize the IV-RMSE relevant to both SPX options and VIX options. Previously, this type of approach could not be tried because the absence of pricing formulas and the notion of the implied volatility for VIX options restricted the opportunity to try this type of approach.

By minimizing the loss function $L^{\mathcal{V}}$, we achieve the various estimates for the hidden states, the parameters, and the $\mathcal{V}$-RMSEs. Moreover, to obtain the standard errors and correlations of the parameter estimates, we derive the variance–covariance matrices of the point estimates using the inverse Hessian for the square of $L^{\mathcal{V}}$ in (12). Under the SV1, z_i is uniquely determined by the relationship (9) between the model and the VIX. By contrast, under the SV2, y_i and z_i cannot be uniquely determined by (9), which is why we also minimize the daily objective with respect to y_i and z_i for each ith date. The daily optimization requires large computational resources. Thus, the calibrations for both models are implemented based on C++ and OpenMP and executed in parallel on 40 CPU cores of two Intel Xeon Gold 6230. The calibrations to the big data are finished within several hours for both the models, which would be virtually impossible without their analytic formulas. In addition, the constrained optimization by linear approximations (COBYLA) algorithm (Powell, 1998) in the NLOPT nonlinear-optimization package (Johnson, 2014) is utilized to find an optimal point of the loss function.

Table 2 shows the estimates, their standard errors and correlations for the parameters, and the $\mathcal{V}$-RMSEs of the models when $\beta_s = 1$ and $\beta_v = 0.0002$ in (13). The SV2 reduces the errors on the test sets of the SPX and the VIX options

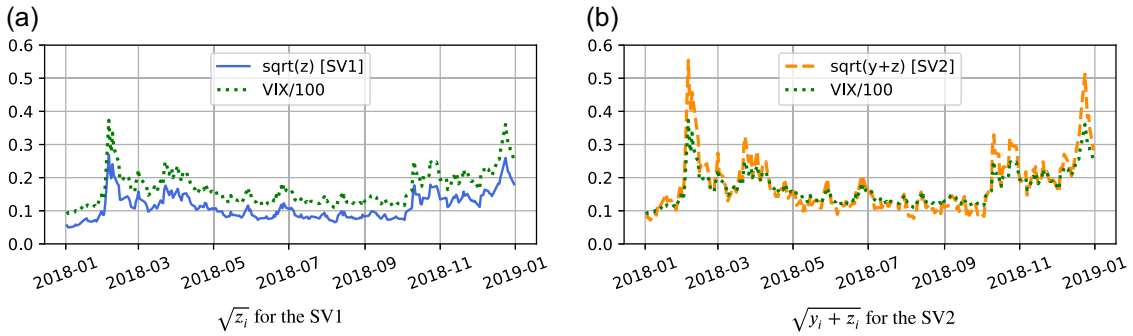

FIGURE 3 Spot volatilities of both models during the period of the test data (2016–2018) (a) $\sqrt{z_i}$ for the SV1; (b) $\sqrt{y_i + z_i}$ for the SV2. SV, stochastic volatility [Color figurecan be viewed at wileyonlinelibrary.com]

TABLE 3 The means and *SD* about the absolute vega errors during the period of the test data

	$\tau < 0.05$			$0.05 \le \tau < 0.1$			$0.1 \le \tau < 0.2$		
	SV1	**SV2**	**Ratio (%)**	**SV1**	**SV2**	**Ratio (%)**	**SV1**	**SV2**	**Ratio (%)**
SPX	0.0335	0.0315	94.2	0.0337	0.0277	82.1	0.0342	0.0280	81.8
	(0.0315)	(0.0308)		(0.0301)	(0.0212)		(0.0301)	(0.0198)	
VIX	0.1113	0.0974	87.5	0.0706	0.0557	78.8	0.0657	0.0534	81.3
	(0.1263)	(0.1026)		(0.0824)	(0.0469)		(0.0759)	(0.0439)	
	$0.2 \le \tau < 0.5$			$\tau \ge 0.5$			**total**		
	SV1	**SV2**	**Ratio (%)**	**SV1**	**SV2**	**Ratio (%)**	**SV1**	**SV2**	**Ratio (%)**
SPX	0.0338	0.0289	85.5	0.0374	0.0331	88.6	0.0336	0.0292	86.7
	(0.0282)	(0.0200)		(0.0295)	(0.0230)		(0.0306)	(0.0254)	
VIX	0.0572	0.0489	85.4	0.0451	0.0434	96.3	0.0776	0.0629	81.0
	(0.0613)	(0.0391)		(0.0293)	(0.0276)		(0.0928)	(0.0623)	

Note: The mean and *SD*, about the absolute vega errors $|e_{ij}|$ during the period of the test data when $\beta_s = 1$ and $\beta_v = 0.0002$ in (13). The results are shown separately by time to maturity τ. The ratio means the value obtained by dividing the error for the SV2 by the corresponding error for the SV1.

Abbreviations: SPX, Standard & Poor's 500 Index; SV, stochastic volatility; VIX, Volatility Index.

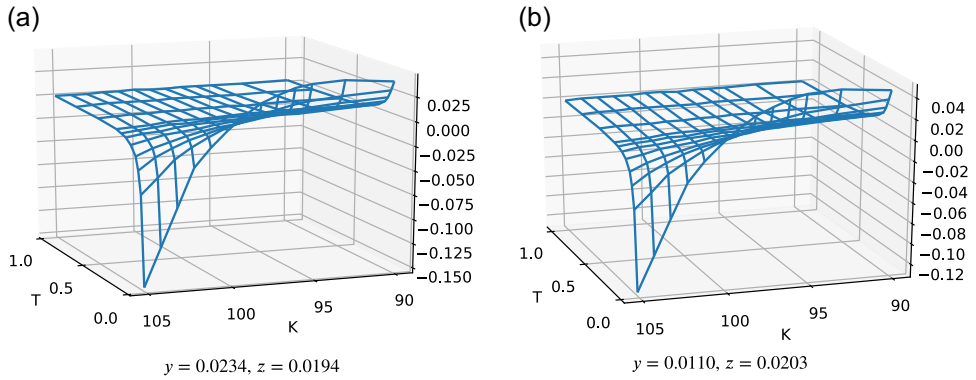

FIGURE 4 Two differences between the Standard & Poor's 500 Index implied volatility surfaces from the corrected and uncorrected prices. Here, $z = 0.0197$ for the uncorrected case (a) $y = 0.0234, z = 0.0194$; (b) $y = 0.0110, z = 0.0203$ [Color figurecan be viewed at wileyonlinelibrary.com]

by 15.5% and 23.72%, respectively, from the SV1. As expected, ϵ and W_3 for the SV2 are so small even if taking their standard errors into consideration, and both time scales are well separated, as $\kappa = 1.49$ and $1/\epsilon = 40.82$. On the other hand, it seems that multicollinearity between the three parameters κ, θ, and σ may exist for both the models. In fact, neglecting long term structure of volatility, increasing both of the mean-reverting rate κ and volatility of volatility σ brings a similar effect with decreasing the long term variance θ. Therefore, including long-term options of which prices are more sensitive to θ can rectify the problem. We leave the problem as further work.

Figure 2 compares the daily errors of the SV1 and SV2 during the period of the test data. The left and right figures indicate the errors for the SPX options and the VIX options, respectively. At first glance, the SV2 produces fewer errors, and it is more robust than the SV1. In particular, the SV1 gives fairly large errors for specific dates. We can postulate a plausible reason for those phenomena from Figure 3, which draws the spot volatilities of both models during the period of the test data. In the figure, the hidden process for the SV2 appears to be more dynamic than that for the SV1. This is because the spot volatility $\sqrt{z_i}$ for the SV1 is strongly correlated with the VIX but $\sqrt{y_i + z_i}$ for the SV2 is not. The SV2 captures short-term volatility that is difficult to detect and produces a more volatile process fluctuating around the VIX. If the SV2 is assumed to be correct, we conclude that the spot volatilities for the SV1 are fairly often biased, especially when sudden strong shocks impact the market. The bias eventually results in large fitting or prediction errors of the SV1 for short-term products, as shown in Table 3. The table sums up the statistics about the absolute vega errors $|e_{i,j}|$ separately by time to maturity. The results in the table confirm that the SV2 performs better than the SV1 as the time to maturity for an option becomes shorter, provided that the time to expiration is not too short. Note that the asymptotic method is valid when the time to maturity is not too short.

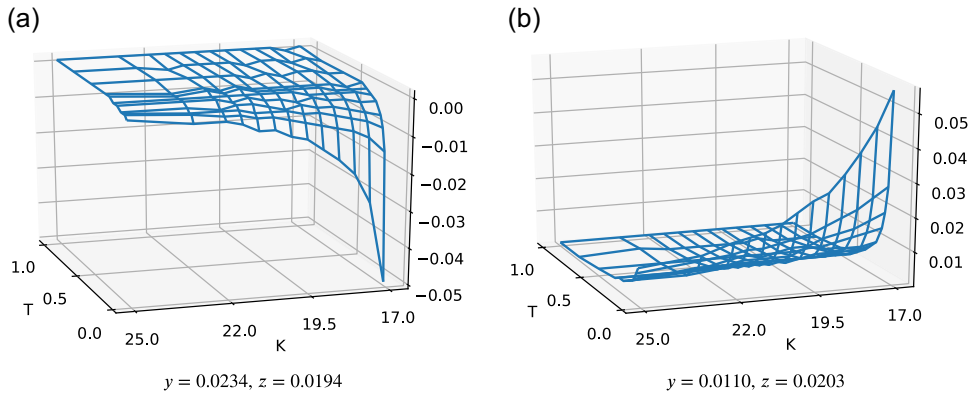

FIGURE 5 Two differences between the Volatility Index implied volatility surfaces from the corrected and uncorrected prices (a) $y = 0.0234, z = 0.0194$; (b) $y = 0.0110, z = 0.0203$ [Color figurecan be viewed at wileyonlinelibrary.com]

Furthermore, implied volatility surfaces for SPX options and VIX options clearly show how appropriate the SV2 is for fitting to short-term products. We now generate implied volatility surfaces $\sigma_{0,1}^{imp}$ from the corrected prices $P_{s,0}(z) + \sqrt{\epsilon} P_{s,1}(z)$ and $P_{v,0}(z) + \epsilon P_{v,1}(y, z)$ with the parameters $\kappa = 3.58, \theta = 0.021\sigma = 0.347, \rho = -1, \epsilon = 0.0096$, and $W_3^{\epsilon} = 0.0150$ for two hidden states $(y, z) = (0.0234, 0.0194)$ and $(y, z) = (0.0110, 0.0203)$. We also generate an additional implied volatility surface σ_0^{imp} from the uncorrected prices $P_{s,0}(z)$ and $P_{v,0}(z)$ for hidden state $z = 0.0197$, which is equivalent to generating the surface using the corrected prices with the same parameters as the preceding case but $\epsilon = 0$ and $W_3^{\epsilon} = 0$. All the hidden states y, z are chosen so that the model value of the VIX is 20, that is, $\text{VIX}_t = 20$ in the relationship (6).

Figures 4 and 5 present the differences $\sigma_{0,1}^{imp} - \sigma_0^{imp}$ for the SPX cases and the VIX cases, respectively. The figures confirm once again that the corrected terms $P_{s,1}$ and $P_{v,1}$ allow excellent short-term flexibility, and thereby capture the fluctuations in the slope and the level of the volatility smirk. Based on Figure 4, $P_{s,1}$ may make short-term in-the-money (SITM) options more expensive than short-term out-of-the-money (SOTM) options in a somewhat robust way. However, based on Figure 5, a subtle change of z in the SV2 seems to lead to a significantly different short-term VIX market. When the short-term state y is smaller than the midterm state z, as in the right figure, $P_{v,1}$ makes the SITM options more expensive than the SOTM options, as in the SPX cases, while $P_{v,1}$ works in the opposite way when y is larger than z, as in the left figure. These phenomena for VIX volatility surfaces may occur because Y_t will be fast oscillating around Z_t in the SV2. If $y > z$, the spot volatility might decline in the short term, which means that the VIX SITM calls would probably not be exercised. If $y < z$, the spot volatility might increase for a short while, which would increase the value of the VIX SOTM call. This is simply the mechanism of the SV2 showing diverse expression for the short-term VIX market in spite of the constraint (6).

5 | CONCLUDING REMARKS

In this paper, we study consistent and efficient pricing of SPX and VIX options under a new two-factor stochastic volatility model. Specifically, this two-factor stochastic volatility model is proposed by adding a fast mean-reverting factor into the Heston model. Doing so facilitates the joint pricing of the SPX option and the VIX option. In practice, joint modeling of both options is important, because an arbitrage relationship exists between the SPX option market and the VIX option market. Moreover, joint modeling leads to a calibration based on extensive market data, including SPX data and VIX data. Since our analytic solutions are derived as one-dimensional integrals, it is obvious that the pricing solutions are computationally very efficient. Our experiment using hundreds of thousands of options shows that the model considerably reduces the errors, compared to a single-scale model. The error reduction is possible because the additional factor reflects short-term impacts in the market, which is difficult to achieve with only one factor for volatility.

In fact, nonaffine models have been less studied for explicit pricing formulas because the involved problems are hard to solve. But the models are more suitable to express actual dynamics (see Kaeck & Alexander, 2013; Mencia & Sentana, 2013, and Yang & Kanniainen, 2017). In this context, our models should be extended to have a nonaffine form. We leave the topic as future work.

ACKNOWLEDGMENTS

Jaegi Jeon received financial support from the National Research Foundation of Korea (NRF) of the Korean government (Grant No. NRF-2019R1I1A1A01062911). Geonwoo Kim received financial support from the NRF (Grant No. NRF-2017R1E1A1A03070886). Jeonggyu Huh received financial support from the NRF (Grant No. NRF-2019R1F1A1058352). The National Research Foundation of Korea of the Korean government (Grant No's. NRF-2019R1I1A1A01062911, NRF-2017R1E1A1A03070886, and NRF-2019R1F1A1058352).

DATA AVAILABILITY STATEMENT

The data employed in this study are available from the CBOE. The SPX and VIX option data sets can be acquired by paying a license fee or under permission.

ORCID

Jeonggyu Huh http://orcid.org/0000-0002-2323-3128

REFERENCES

Bayer, C., Gatheral, J., & Karlsmark, M. (2013). Fast ninomiya-victoir calibration of the double-mean-reverting model. *Quantitative Finance*, *13*, 1813–1829.

Brigo, D., & Mercurio, F. (2007). *Interest rate models-theory and practice: with smile, inflation and credit*. Springer Science & Business Media.

Broadie, M., Chernov, M., & Johannes, M. (2007). Model specification and risk premia: Evidence from futures options. *The Journal of Finance*, *62*, 1453–1490.

Carr, P., & Madan, D. (1998). Towards a theory of volatility trading. *Volatility: New Estimation Techniques for Pricing Derivatives*, *29*, 417–427.

Cheng, J., Ibraimi, M., Leippold, M., & Zhang, J. E. (2012). A remark on Lin and Chang's paper 'consistent modeling of S&P 500 and vix derivatives. *Journal of Economic Dynamics and Control*, *36*, 708–715.

Chernov, M., Gallant, A. R., Ghysels, E., & Tauchen, G. (2003). Alternative models for stock price dynamics. *Journal of Econometrics*, *116*, 225–257.

Christoffersen, P., Heston, S., & Jacobs, K. (2009). The shape and term structure of the index option smirk: Why multifactor stochastic volatility models work so well. *Management Science*, *55*, 1914–1932.

Cont, R., & Kokholm, T. (2013). A consistent pricing model for index options and volatility derivatives. *Mathematical Finance: An International Journal of Mathematics Statistics and Financial Economics*, *23*, 248–274.

Duffie, D., Pan, J., & Singleton, K. (2000). Transform analysis and asset pricing for affine jump-diffusions. *Econometrica*, *68*, 1343–1376.

Fouque, J.-P., & Lorig, M. J. (2011). A fast mean-reverting correction to Heston's stochastic volatility model. *SIAM Journal on Financial Mathematics*, *2*, 221–254.

Fouque, J.-P., Papanicolaou, G., Sircar, R., & Sølna, K. (2011). *Multiscale stochastic volatility for equity, interest rate, and credit derivatives*. Cambridge University Press.

Fouque, J.-P., & Saporito, Y. F. (2018). Heston stochastic vol-of-vol model for joint calibration of VIX and S&P 500 options. *Quantitative Finance*, *18*, 1003–1016.

Gallant, A. R., Hsu, C.-T., & Tauchen, G. (1999). Using daily range data to calibrate volatility diffusions and extract the forward integrated variance. *Review of Economics and Statistics*, *81*, 617–631.

Gatheral, J. (2008). *Consistent modeling of SPX and VIX options* (Vol. 3). Bachelier Congress.

Huh, J., Jeon, J., & Kim, J.-H. (2018). A scaled version of the double-mean-reverting model for VIX derivatives. *Mathematics and Financial Economics*, *12*, 495–515.

Johnson, S. G. (2014). The NLopt nonlinear-optimization package [software]. http://github.com/stevengj/nlopt

Kaeck, A., & Alexander, C. (2012). Volatility dynamics for the S&P 500: Further evidence from non-affine, multi-factor jump diffusions. *Journal of Banking & Finance*, *36*, 3110–3121.

Kaeck, A., & Alexander, C. (2013). Continuous-time VIX dynamics: On the role of stochastic volatility of volatility. *International Review of Financial Analysis*, *28*, 46–56.

Lian, G -H., & Zhu, S.-P. (2013). Pricing VIX options with stochastic volatility and random jumps. *Decisions in Economics and Finance*, *36*, 71–88.

Lin, Y.-N., & Chang, C.-H. (2009). VIX option pricing. *Journal of Futures Markets: Futures, Options, and Other Derivative Products*, *29*, 523–543.

Lin, Y. -N., & Chang, C.-H. (2010). Consistent modeling of S&P 500 and VIX derivatives. *Journal of Economic Dynamics and Control*, *34*, 2302–2319.

Mencia, J., & Sentana, E. (2013). Valuation of VIX derivatives. *Journal of Financial Economics*, *108*, 367–391.

Powell, M. J. (1998). Direct search algorithms for optimization calculations. *Acta Numerica*, *7*, 287–336.

SPX data. S&P Dow Jones Indices; 2016-2018; S&P 500. https://www.spglobal.com

SPX and VIX option data. CBOE; 2016–2018; End-of-day option quotes data. https://datashop.cboe.com

VIX data. CBOE; 2016–2018; VIX historical price data. https://ww2.cboe.com

VIX future data. CBOE; 2016–2018; CBOE volatility index (VX) futures, includes TAS. https://markets.cboe.com

Yang, H., & Kanniainen, J. (2017). Jump and volatility dynamics for the S&P 500: Evidence for infinite-activity jumps with non-affine volatility dynamics from stock and option markets. *Review of Finance*, *21*, 811–844.

How to cite this article: Jeon J, Kim G, Huh J. Consistent and efficient pricing of SPX and VIX options under multiscale stochastic volatility. *J Futures Markets*. 2021;41:559–576. https://doi.org/10.1002/fut.22190

APPENDIX A: DERIVATION OF ANALYTIC FORMULA FOR SPX OPTIONS

Putting $P_s^\epsilon = P_{s,0} + \sqrt{\epsilon}P_{s,1} + \epsilon P_{s,2} + \epsilon\sqrt{\epsilon}P_{s,3} + \cdots$ into the PDE (3),

$$\frac{1}{\epsilon}\mathcal{L}_{s,0}P_{s,0} + \frac{1}{\sqrt{\epsilon}}(\mathcal{L}_{s,0}P_{s,1} + \mathcal{L}_{s,1}P_{s,0}) + (\mathcal{L}_{s,0}P_{s,2} + \mathcal{L}_{s,1}P_{s,1} + \mathcal{L}_{s,2}P_{s,0}) + \sqrt{\epsilon}(\mathcal{L}_{s,0}P_{s,3} + \mathcal{L}_{s,1}P_{s,2} + \mathcal{L}_{s,2}P_{s,1}) + \cdots = 0.$$

As mentioned in Theorem 1, we intend for the sum of the leading term $P_{s,0}$ and the first non-zero correction term $P_{s,1}$ to approximate P_s^ϵ within accuracy $O(\epsilon)$, that is, $\left|P_s^\epsilon - (P_{s,0} + \sqrt{\epsilon}P_{s,1})\right| < C\epsilon$ for some positive C. For this purpose, the following equations should be satisfied:

$$\mathcal{L}_{s,0}P_{s,0} = 0, \tag{A1}$$

$$\mathcal{L}_{s,0}P_{s,1} + \mathcal{L}_{s,1}P_{s,0} = 0, \tag{A2}$$

$$\mathcal{L}_{s,0}P_{s,2} + \mathcal{L}_{s,1}P_{s,1} + \mathcal{L}_{s,2}P_{s,0} = 0, \tag{A3}$$

$$\mathcal{L}_{s,0}P_{s,3} + \mathcal{L}_{s,1}P_{s,2} + \mathcal{L}_{s,2}P_{s,1} = 0. \tag{A4}$$

$P_{s,0}$ should not depend on y so that the Poisson equation (A1) has a solution. This means that $P_{s,1}$ also does not depend on y owing to (A2). From (A3), we then obtain

$$\mathcal{L}_{s,0}P_{s,2} + \mathcal{L}_{s,2}P_{s,0} = 0. \tag{A5}$$

Thus, the centering condition for $\mathcal{L}_{s,0}$ for the Poisson equation (A5) results in the following PDE (4) for $P_{s,0}$:

$$\begin{aligned} \langle\mathcal{L}_{s,2}P_{s,0}\rangle &= \langle\mathcal{L}_{s,2}\rangle P_{s,0} = 0, \\ P_{s,0}(T,x,z) &= (x-K)^+, \end{aligned} \tag{A6}$$

where $\langle\cdot\rangle$ is the expectation with respect to the invariant distribution Φ for Y_t. The centering condition indicates that $\langle g\rangle = 0$ should hold for Poisson equation $\mathcal{L}f + g = 0$. The condition is necessary for a Poisson equation to have a solution.

In addition, (A5) yields the following equation:

$$\begin{aligned} P_{s,2} &= -\mathcal{L}_{s,0}^{-1}(\mathcal{L}_{s,2} - \langle\mathcal{L}_{s,2}\rangle)P_{s,0} + c(t,x,z) \\ &= -\frac{1}{2}x^2\phi(y,z)\partial_{xx}^2 P_{s,0} + c(t,x,z), \end{aligned} \tag{A7}$$

where

$$\mathcal{L}_{s,0}\phi(y,z) = y - z. \tag{A8}$$

In fact, we show $\phi(y,z) = z - y$, the proof of which is given in B. On one hand, if we put (A7) into (A4) and use the centering condition for $\mathcal{L}_{s,0}$ in (A4), we achieve the PDE (5) for $P_{s,1}$ in the following ways:

$$\begin{aligned} \langle\mathcal{L}_{s,2}\rangle P_{s,1} &= -\langle\mathcal{L}_{s,1}P_{s,2}\rangle \\ &= \frac{1}{\sqrt{2}}\eta\nu\langle y\phi_y(y,z)\rangle x\partial_x\left(x^2\partial_{xx}^2 P_0\right) \\ &= W_3 z x\partial_x\left(x^2\partial_{xx}^2\right)P_{s,0}. \end{aligned} \tag{A9}$$

with the corresponding final condition

$$P_{s,1}(T,x,z) = 0,$$

where $W_3 = -\frac{1}{\sqrt{2}}\eta\nu$ (recall that $W_3^\epsilon = -\frac{1}{\sqrt{2}}\eta\nu\sqrt{\epsilon}$, i.e., $W_3 = W_3^\epsilon/\sqrt{\epsilon}$).

On the other hand, if $\xi := 2z$, Equations (A6) and (A9) are transformed as follows, and they are associated with the PDE operator $\mathcal{L}_H$ for the Heston model, whose parameters are the mean reversion rate of κ, the long-run variance 2θ, the volatility of variance $\sqrt{2}\sigma$, and the correlation $\sqrt{2}\rho$ between stock price and its variance.

$$\begin{aligned}\mathcal{L}_H \tilde{P}_{s,0}(t,x,\xi) &= 0,\\ \mathcal{L}_H \tilde{P}_{s,1}(t,x,\xi) &= \frac{1}{2}W_3\xi x\partial_x\left(x^2\partial^2_{xx}\right)\tilde{P}_{s,0}(t,x,\xi),\end{aligned} \tag{A10}$$

where

$$\mathcal{L}_H = \partial_t + rx\partial_x + \kappa(2\theta-\xi)\partial_\xi + \frac{1}{2}x^2\xi\partial^2_{xx} + \frac{1}{2}(\sqrt{2}\sigma)^2\xi\partial^2_{\xi\xi} + \left(\frac{1}{\sqrt{2}}\rho\right)(\sqrt{2}\sigma)x\xi\partial^2_{x\xi} - r.$$

Similar to Fouque and Lorig (2011), by utilizing the feasibility of the Heston model, we can achieve the following solutions of the abovementioned PDEs:

$$\begin{aligned}\tilde{P}_{s,0}(t,x,\xi) &= \frac{e^{-r\tau}}{2\pi}\int e^{-ikq}\hat{G}(\tau,k,2\xi)\hat{h}(k)dk,\\ \tilde{P}_{s,1}(t,x,\xi) &= \frac{e^{-r\tau}}{2\pi}\int e^{-ikq}b(k)(\kappa\theta\hat{f}_0(\tau,k) + 2z\hat{f}_1(\tau,k))\hat{G}(\tau,k,\xi)\hat{h}(k)dk,\end{aligned}$$

where $\tau = T-t, q = r\tau + \log x$,

$$\begin{aligned}b(k) &= -\frac{1}{2}W_3(ik^3+k^2),\\ \hat{f}_0(\tau,k) &= \int_0^\tau \hat{f}_1(t,k)dt,\\ \hat{f}_1(\tau,k) &= \int_0^\tau\left(\frac{g(k)e^{sd(k)}-1}{g(k)e^{\tau d(k)}-1}\right)^2 e^{d(k)(\tau-s)}ds,\end{aligned}$$

and $\hat{G}(\tau,k,z), \hat{h}(k), d(k)$, and $g(k)$ are defined in Theorem 1. To compute $\tilde{P}_{s,0}$ and $\tilde{P}_{s,1}$, numerical integrations need to be associated with a single integration and a triple integration. However, as in the foregoing discussion in 3.1, numerical methods for the triple integration are too computationally intensive. Fortunately, we can further simplify $\hat{f}_0$ and $\hat{f}_1$, because the right-hand side of (A10) is linear with respect to ξ. The induction process is given in detail as follows:

$$\begin{aligned}\hat{f}_1(\tau,k) &= \int_0^\tau \frac{(g(k)e^{sd(k)}-1)^2}{(g(k)e^{\tau d(k)}-1)^2}e^{d(k)(\tau-s)}ds\\ &= \frac{e^{\tau d(k)}}{(g(k)e^{\tau d(k)}-1)^2}\int_0^\tau \frac{(g(k)e^{sd(k)}-1)^2}{e^{sd(k)}}ds\\ &= \left(\frac{e^{\tau d(k)}}{(g(k)e^{\tau d(k)}-1)^2}\right)\left(\frac{1}{d(k)}(g(k)^2e^{\tau d(k)} - 2\tau d(k)g(k) - e^{-\tau d(k)} + 1 - g(k)^2)\right) + 1\\ &= \frac{e^{\tau d(k)}(g(k)^2(e^{\tau d(k)}-1) - 2\tau d(k)g(k) + 1) - 1}{d(k)(g(k)e^{\tau d(k)}-1)^2}.\end{aligned}$$

If $I(\tau,k) \coloneqq \frac{e^{\tau d(k)}}{(g(k)e^{\tau d(k)}-1)^2}$, $\hat{f}_1(\tau,k) = I(t,k)\int_0^t \frac{1}{I(s,k)}ds$ from the second line of the above equations. Thus, we can obtain

$$\begin{aligned}\hat{f}_0(\tau,k) &= \int_0^\tau I(t,k)\int_0^t \frac{1}{I(s,k)}dsdt\\ &= \int_0^\tau \frac{1}{I(s,k)}\int_s^\tau I(t,k)dtds\\ &= \int_0^\tau \frac{(g(k)e^{sd(k)}-1)^2}{e^{sd(k)}}\left(\frac{1}{d(k)g(k) - d(k)g(k)^2e^{\tau d(k)}} - \frac{1}{d(k)g(k) - d(k)g(k)^2e^{sd(k)}}\right)ds\\ &= \frac{2\tau d(k)g(k) + g^2(k) - 1}{d^2(k)g(k)(g(k)e^{\tau d(k)}-1)} + \frac{\tau d(k)g(k) - g(k) - 1}{d^2(k)g(k)}.\end{aligned}$$

APPENDIX B: SOLUTION FOR POISSON EQUATION (A8)

By the spectral theory, solution ϕ for Poisson equation (A8) can be found as follows:

$$\phi(y,z) = z - y.$$

Now, we briefly explain the way to find ϕ. It is known that the operator $\mathcal{L}_{s,0}$ has the eigenvalues $\lambda_n = -n (n \in \mathbb{N})$ and the family of eigenfunctions ψ_n associated with eigenvalue λ_n (i.e., $\mathcal{L}_{s,0}\psi_n = \lambda_n \psi_n$) is

$$\psi_n(y) = \sqrt{\frac{n!\Gamma(\gamma)}{\Gamma(n+\gamma)}} L_n\left(\frac{y}{\nu^2}\right),$$

where $\gamma = \frac{z}{\nu^2}$ and L_n is an n-order Legendre polynomial, that is, $L_n(w) = \frac{w^{1-\gamma}e^w}{n!}\frac{d^n}{dw^n}(w^{n+\gamma-1}e^{-w})$. It is also known that ψ_n form a complete orthogonal basis of the Hilbert space $L^2(\Phi)$. Φ is the invariant distribution of Y_t, which is defined in the foregoing section. Thus, $y - z \in L^2(\Phi)$ can be expressed as follows:

$$y - z = \sum_{n\geq 0} c_n \psi_n(y), \tag{B1}$$

where $c_n = \langle (y-z)\psi_n \rangle$. For any n, c_n are explicitly calculated as follows:

$$c_n = \begin{cases} -\nu\sqrt{z} & \text{if} \quad n = 1 \\ 0 & \text{otherwise} \end{cases} \tag{B2}$$

We provide the induction process for the above formula (B2). First, c_0 can be easily obtained as follows:

$$c_0 = \langle (y-z)\psi_0 \rangle = \langle y - z \rangle = 0.$$

In addition, c_1 is computed as follows:

$$\begin{aligned} c_1 &= \langle (y-z)\psi_1 \rangle \\ &= \sqrt{\frac{\Gamma(\gamma)}{\Gamma(1+\gamma)}} \int_0^\infty (y-z)\left(\gamma - \frac{y}{\nu^2}\right)\Phi(y)dy \\ &= \sqrt{\frac{1}{\gamma}} \int_0^\infty \left(-\frac{1}{\nu^2}y^2 + \left(\frac{z}{\nu^2} + \gamma\right)y - \gamma z\right)\Phi(y)dy \\ &= -\nu\sqrt{z}. \end{aligned}$$

It is also proved that c_n for $n \geq 2$ are zero, because we can show the following equation:

$$\begin{aligned} & \int_0^\infty y\left[\left(\frac{y}{\nu^2}\right)^{1-\gamma} e^{\frac{y}{\nu^2}} \frac{d^n}{dy^n}\left(\left(\frac{y}{\nu^2}\right)^{n+\gamma-1} e^{-\frac{y}{\nu^2}}\right)\right]\left[y^{\gamma-1}e^{-(y/\nu^2)}\right] dy \\ = \; & \nu^{2\gamma-2}\int_0^\infty y \frac{d^n}{dy^n}\left(\left(\frac{y}{\nu^2}\right)^{n+\gamma-1} e^{-\frac{y}{\nu^2}}\right)dy \\ = \; & -\nu^{2\gamma-2}\int_0^\infty \frac{d^{n-1}}{dy^{n-1}}\left(\left(\frac{y}{\nu^2}\right)^{n+\gamma-1} e^{-\frac{y}{\nu^2}}\right)dy \\ = \; & -\nu^{2\gamma-2}\left[\frac{d^{n-2}}{dy^{n-2}}\left(\left(\frac{y}{\nu^2}\right)^{n+\gamma-1} e^{-\frac{y}{\nu^2}}\right)\right]_0^\infty \\ = \; & \nu^{2\gamma-2}\left[(n+\gamma-1) \quad \text{th degree polynomial without constant term} \times e^{-\frac{y}{\nu^2}}\right]_0^\infty \\ = \; & 0. \end{aligned}$$

Therefore, we eventually obtain the following ϕ by (B1) and (B2):

$$\begin{aligned}\phi(y,z) &= \frac{c_1\psi_1(y)}{\lambda_1}\\ &= \frac{z}{\gamma}\left(\gamma - \frac{y}{\nu^2}\right)\\ &= z - y.\end{aligned}$$